Journal Pre-proofs

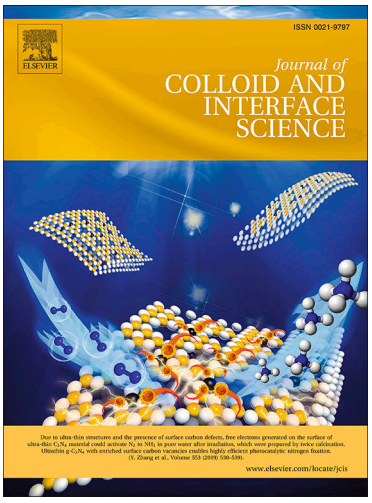

Interpreting Rheology and Electrical conductivity: it all boils down to which particle size

Robinson C.D. Cruz, Ana M. Segadães, Pedro Q. Mantas, Rainer Oberacker, Michael J. Hoffmann

PII: S0021-9797(20)30494-X
DOI: https://doi.org/10.1016/j.jcis.2020.04.046
Reference: YJCIS 26287

To appear in: *Journal of Colloid and Interface Science*

Received Date: 17 January 2020
Revised Date: 9 April 2020
Accepted Date: 10 April 2020

Please cite this article as: R.C.D. Cruz, A.M. Segadães, P.Q. Mantas, R. Oberacker, M.J. Hoffmann, Interpreting Rheology and Electrical conductivity: it all boils down to which particle size, *Journal of Colloid and Interface Science* (2020), doi: https://doi.org/10.1016/j.jcis.2020.04.046

Interpreting Rheology and Electrical conductivity: it all boils down to which particle size

Robinson C. D. Cruz [a], Ana M. Segadães [b,c] *, Pedro Q. Mantas [b], Rainer Oberacker [d], Michael J. Hoffmann [d]

[a] University of Caxias do Sul, IMC–Instituto de Materiais Cerâmicos, Bom Princípio, Brazil

[b] University of Aveiro, Department of Materials and Ceramics Engineering, Aveiro, Portugal

[c] University of Aveiro, CICECO–Aveiro Institute of Materials, Aveiro, Portugal

[d] Karlsruhe Institute of Technology, Institute for Applied Materials, Ceramics in Mechanical Engineering, Karlsruhe, Germany

Graphical abstract

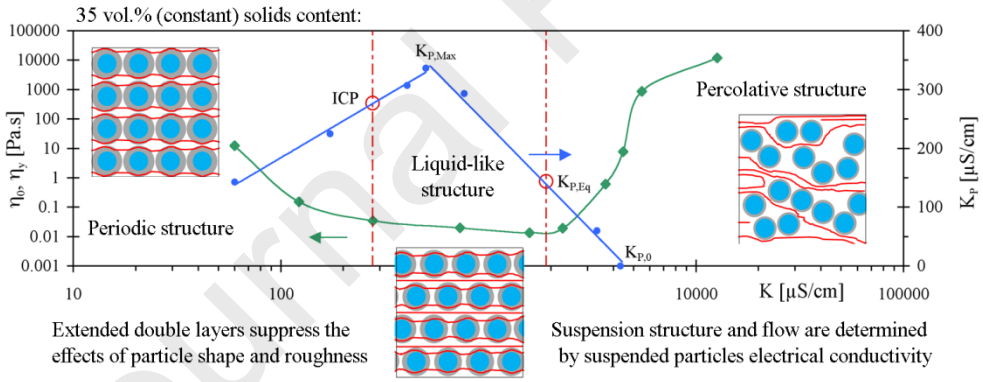

Highlights:

1) New approach to the relationships between structure and stability of suspensions
2) Suspension structure determined by suspended particles electrical conductivity
3) Periodic, liquid-like and percolative structures for a constant solids content
4) Expanded double layers suppress the effects of particle shape and roughness
5) Surface area particle radius enables tuning of rheological models for hard spheres

* Corresponding author. Phone: +351 234 370 236; e-mail: segadaes@ua.pt

Abstract

Hypothesis: The electrical charges that develop on the surface of the ceramic particles upon contact with water, due to the interaction with ions in solution, result in a liquid-solid interface, which utterly modifies the properties of individual particles and the way they interact with each other to form a structure. This work explores a new approach to the relationships between structure and stability of suspensions. Experiments: For this purpose, suspensions with a constant 0.35 volume fraction of α-alumina particles, neither spherical nor smooth, and controlled ionic strength (0-90 mM KCl) were prepared and characterized in terms of flow behaviour, electrical conductivity and particle's electrokinetic mobility. Findings: Electrical conductivity (132 μS/cm < conductivity < 5730 μS/cm) and rheology measurements (10^{-2} Pa.s < viscosity < 10^{4} Pa.s) were found to complement each other to produce a more accurate picture of the suspension's structure. Deviations of experimental data from well-accepted behavioural models were elucidated when the surface area equivalent particle size was used. With the electrical double layer thickness obtained from electrical conductivity measurements, this enabled the interpretation of the relationship between the suspension's viscosity and the particles electrical conductivity, which provides a criterion for the stability of concentrated colloidal suspensions.

KEYWORDS: Rheology; Viscosity; Suspension electrical conductivity; Zeta-potential; Alumina particle; DLVO; Colloidal interactions.

1. INTRODUCTION

Many industrial applications rely on the ability to manipulate the flow behaviour (rheology) of colloidal suspensions, especially at high solids contents. The increase in the fluid viscosity that results from the addition of particles to a suspending liquid (continuous fluid phase) is generally accompanied by a deviation from the Newtonian behaviour that the simple hydrodynamic disturbance of the flow fails to explain. At moderate solids volume fraction, aqueous colloidal suspensions generally flow like shear-thinning low viscosity liquids but the effect of shear rate on the viscosity of concentrated suspensions is normally more complex and difficult to explain. At high solids volume fractions, particularly for electrostatically

charged suspended particles, interparticle interactions result in a structural network that may extend over the entire volume of the suspension and give rise to elastic-like and time-dependent behaviours. Generally, a finite applied shear is needed to generate the stress necessary to deform that structural particle network (yield stress) and start suspension flow. Other oddities are commonly attributed to the particles' morphology, namely shape anisotropy and surface roughness [1].

Clearly, under applied (external) shear the suspensions rheological behaviour is a combination of the mechanical response of the continuous suspending liquid and that of the corresponding particle structure. Nevertheless, because the flow characteristic length scale substantially exceeds the particle size and suspensions behave on the macroscale as a continuum, interpretation efforts have generally been aimed at incorporating the latter effect into the existing behavioural models for similar continuous (incompressible) fluids, as summarized in what follows.

Specific models proposed to interpret suspensions rheology began [2] by considering dilute suspensions of spherical particles (minimum hydrodynamic effects) that were smooth (no surface roughness effects) and hard (no surface charge, hence no double layer effects), all having the same size (no particle packing effects).

The Derjaguin–Landau–Verwey–Overbeek (DLVO) theory for the electrostatic interactions between particle pairs introduced in the late 1940s [3, 4] provided the basis to explain the stability and electroviscous effects observed in diluted suspensions demonstrating that, for the same particle system, the nature of the structure that develops in the suspension depends on the characteristics of the suspending liquid. According to the DLVO theory, suspended particles can lie on a dominant repulsive or attractive equilibrium state, described by a total potential curve with or without a secondary minimum. Both the particles total electrostatic potential and the thickness κ^{-1} of their electrical double layer are governed by the ionic strength of the suspending liquid. The range of electrostatic interaction is judged by κa, where a is the radius of the solid particle. For dominant repulsive forces (electrostatic in this case, or steric as realised later), particles tend to stand at an equilibrium distance, giving rise to a periodic structure detectable by optical methods, whereas a percolative structure results from dominant attractive forces [5, 6].

On the other hand, in a flowing suspension of electrostatically charged particles, each moving particle drags with it its electrical double layer (excluded volume) and its electrokinetic potential is represented by zeta-potential (ζ-potential), which is supposedly measured at the outer limit (shear plane) of the double layer. Thus, the hard, smooth spheres with no surface charge, considered in the original models, could be replaced by soft spheres with surface charge and electrical double layers (or with adsorbed polymers) whose thickness is inferred from ζ-potential measurements. Added ions (varying ionic strength) explain the reduction in the thickness κ^{-1} of the electrical double layer, which, in turn, explains the reduction in the viscosity that occurs after the suspensions begin to flow. Such effects were also included in the models [7].

Although interparticle forces are short ranged and decrease in magnitude with increasing particle separation, as the particles volume fraction ϕ increases the particle structure that forms in the suspension can no longer be dismissed. That particle structure, whether it is periodic or percolative, can extend over the entire volume of the suspension or be restricted to sedimented individual particles or flocs thereof and its effect, as well as that of the maximum particle volume fraction ϕ_{Max}, should also be included in the models [8, 9]. Attractive volume filling structures confine part of the continuous phase, which translates into larger effective particle volume fraction ϕ_{eff} and results in increased viscosity. Repulsive volume filling structures also define an excluded volume, which is not accessible by another particle, leading to the development of a crystalline or gel-like state at particle concentrations lower than the expected maximum packing fraction, ϕ_{Max} [6, 10, 11]. The concept of effective particle volume fraction ϕ_{eff} can also be used to account for the increase in the hydrodynamic particle radius due to the double layer thickness: for a given particle radius *a*, the thicker the electrical double layer, the larger the excluded volume and the effective solids volume fraction [12].

Such amendments should suffice to embody the mechanical response of the particle structure in the suspension, so that the suspensions rheological behaviour under applied (external) shear might still be interpreted in terms similar to those used for the behaviour of continuous fluids, which are briefly described next.

Under stationary conditions (steady-state behaviour), the viscous response of an incompressible fluid describes how the shear stress τ is related to the shear rate $\dot{\gamma}$ through the viscosity η. The latter is a material property that depends on the shear rate. In the simplest

cases (Newtonian behaviour) the viscosity is constant (*i.e.* $\tau = \eta\dot{\gamma}$), but it can be a more complicate function of the shear rate. In such cases (shear-thickening or dilatant, shear-thinning or pseudoplastic, Bingham-plastic and non-linear plastic behaviour), reasoning can be brought back to simplicity by considering an apparent viscosity (constant for each $\dot{\gamma}$, calculated as for the equivalent Newtonion fluid). Experimental τ *vs.* $\dot{\gamma}$ flow curves are usually converted into η *vs.* $\dot{\gamma}$ curves by using the apparent viscosity concept [13, 14]. Care should be taken to remember that, except for Newtonian fluids, these curves are not the representation of the derivative of the τ *vs.* $\dot{\gamma}$ curves (true viscosity). Such artefact in the apparent viscosity curves is at times responsible for Bingham-plastic flows to be mistakenly considered shear-thinning.

The shear-thinning behaviour of highly dispersed suspensions can be regarded as a kinetic process with contributions from, in one hand, the combined effects of Brownian motion (thermal effects) and particle interactions (electrostatic forces) and, on the other, the hydrodynamic forces due to the shear process [11, 15]. At low shear rates, Brownian motion and particle interactions hold the particles in a random arrangement, each individual particle being in an energy minimum generated by the neighbouring particles. At this stage, when disturbed, the particles can quickly move to a new equivalent equilibrium position (because a finite applied shear is generally required before any stress can be measured, this is a time-dependent process known as stress relaxation). When the shear rate balances the Brownian molecular motion and particle interactions, stresses can no longer relax and the particles are turned into the flow direction. That particular shear rate heralds the shear-thinning behaviour and the corresponding apparent viscosity is referred to as zero-shear viscosity (η_0). As the shear rate increases and the liquid confined in the previously excluded volume is progressively made available (as already mentioned, interparticle forces decrease in magnitude with increasing particle separation), viscous flow occurs with a continuous lowering of the viscosity. Eventually, there will be a moment when the hydrodynamic forces dominate particle mobility and the particles are displaced so fast that all structure is lost and a viscosity minimum (η_∞) is reached. The Carreau-Yasuda model [16] proposes a power-law dependence of viscosity on shear and is found to be particularly well suited for the representation of such shear-thinning flow between those limiting viscosities η_0 and η_∞.

For concentrated suspensions that normally exhibit plastic behaviour, flow only occurs when the resulting stress overcomes a clear definite yield stress τ_y (flow limit) and the structure

collapses. Although there is no flow below τ_y, the suspension behaves elastically and a stress can actually be measured. The nature of the particle structure that is present in a concentrated suspension is expected to control both the suspension's flow behaviour after τ_y and the viscoelastic behaviour before τ_y and can be inferred from either.

In terms of flow behaviour, if the slope of the $\tau - \dot{\gamma}$ flow curve remains constant after τ_y, the system is called Bingham-plastic (that constant slope is called plastic viscosity); if the flow curve is non-linear after τ_y, the system is called non-linear plastic with a variable (structural) viscosity. It could be said that the Bingham-plastic flow is a Newtonian one with a flow limit and that the non-linear plastic flow is shear-thinning with a flow limit.

Various models are generally accepted to describe the non-linear plastic flow behaviour of suspensions [14, 17, 18]. The Herschel-Bulkley model ($\tau = \tau_y + k_1 \dot{\gamma}^n$, where k_1 and n are constants) is among the best suited to do it, as it includes the special cases of Bingham flow (in which $n = 1$) and Newtonian flow (when $n = 1$ and $\tau_y = 0$). According to this model, the effect of the suspension's structure can be separated into the initial resistance to start flowing, measured by τ_y, and the flow itself (shear rate power law), measured by k_1 and n. Changes in τ_y can be due to either the interparticle forces or to the degree of linking within the particle network. The parameter k_1 represents the competition between the redispersion of agglomerated particles and the reagglomeration of dispersed particles, *i.e.* k_1 measures the interparticle forces within the agglomerates and represents the colloidal component of the flow response. The parameter n represents the viscous component of the suspension response, hence, the uniformity of shape and size of particle agglomerates ($n < 1$ signals the formation of agglomerates).

There is one final attempt worth mentioning, to explain the movement of particles in a flowing suspension that behaves on the macroscale as a continuum: flow can also be regarded as a transport phenomenon and, as such, be described in a simplified manner by the use of dimensionless numbers [10, 11]. Once the parameters that affect the properties of interest are identified, dimensionless ratios of those physical quantities can provide a basis for assessing the relative importance of individual forces. Since viscous forces act on the particle structure against the restoring effect of Brownian motion, the Péclet number *Pe*, which is the ratio between the convection dominated (or bulk motion) transport rate and the diffusion dominated (or gradient) transport rate, can be used. In the context of mass transfer, *Pe* is the

product of the Reynolds and the Schmidt numbers. Briefly, for suspensions of hard spheres, *Pe* is a linear function of $\dot{\gamma}$, as is the shear stress by means of the apparent viscosity, which means that the curves τ *vs*. $\dot{\gamma}$ and τ *vs*. *Pe* are geometrically similar and can be made to coincide using the appropriate normalization. Comparison of the *Pe vs.* $\dot{\gamma}$ line with actual flow curves readily brings out any departure between the two, if it occurs, which is a tell-tale of the effect of variables other than Brownian molecular motion or the hydrodynamic forces over the flow behaviour. Electrostatically stabilized suspensions (soft sphere particles) typically present a poor correlation with *Pe* [19].

In any case, viscosity relates shear stress to deformation, and it is influenced by the hydrodynamic (viscous) interactions, the Brownian motion and the particle interactions, and depends on the volume fraction of the particles. Since the end of the past century, clear trends have been established for the correlation between the suspension shear viscosity and the particles ζ-potential and electrical double layer thickness κ^{-1}. However, discrepancies and anomalies are still observed while fitting to real suspensions rheology models derived for continuous fluids. The former are often attributed to the deviations from idealized systems, and the ability to anticipate or quantitatively predict rheological responses remains somehow limited [7].

A further complication arises at the nano-size level, as colloidal interactions prevail over hydrodynamics and particles can indeed be regarded as a mere disturbance of the continuous medium that envelops them, rather than the determining variable. The solid particle size loses relevance and both ζ-potential and the electrical double layer of thickness κ^{-1} become properties of the suspending liquid, which "sees" the particles through their surface area. From this point of view, both shape and roughness might be better accounted for in the particle surface area and expressed as an equivalent spherical particle radius a_s [20].

A recent study in the literature [21] showed how the mobility of suspended α-Al_2O_3 particles could be translated into relationships between ζ–potential and electrical conductivity. The use of Maxwell's model enabled the calculation of the particles electrical conductivity K_P, which increased with increasing ionic strength up to a maximum value ($K_{P,Max}$), to decrease again with further salt addition until the particle surface was no longer conductive ($K_{P,0}$). At $K_{P,Max}$ the repulsive potential between particles is maximum (*i.e.* fully expanded double layer) and, therefore, $K_{P,Max}$ can be used to detect the effective beginning of the diffuse layer

compression. As such compression progresses, the shallow secondary attractive minimum predicted by the DLVO theory begins to form, inside which particles can stand closer, while their conductivity decreases. The complete collapse of the double layer occurs at $K_{P,0}$, when particles no longer conduct and stand at the closest distance that prevents falling into the DLVO primary attractive minimum. Therefore, the slightly attractive interparticle equilibrium distance generally associated with electrostatically stabilized suspensions of minimum viscosity (*i.e*. processing window) occurs between particles maximum and zero conductivity, $K_{P,Max}$ and $K_{P,0}$, which can be assessed through the relationships between electrical conductivity and ionic strength. Furthermore, maximum ζ–potential was observed at the isoconductivity point (ICP) between particles and suspending liquid and separates electrical conductivity preferential paths: through the particles electrical double layer (before the ICP), or through the free ions in the suspending liquid (beyond the ICP).

In other words, electrical conductivity measurements brought to light that the increase in the salt concentration not only results in a decrease of ζ-potential but also, and above all, has strong implications in particle stability. Essentially, that work [21] not only showed that a high zeta potential is a necessary but not sufficient condition for the colloidal stability of fine particles, but also provided a different way of picturing the suspensions structure, with important implications in colloidal suspensions manipulation and consolidation methods.

This work further extends that approach into the investigation of the flow behaviour of concentrated colloidal suspensions of α-alumina particles, neither spherical nor smooth, seeking a comprehensive description of the relationships between the mechanical behaviour, the structure and the stability of concentrated suspensions. An interpretation will be sought for the viscoelastic properties of electrostatically stabilized colloidal suspensions in terms of the contribution of the repulsive forces caused by changes in the ionic strength of the suspending liquid, gauged by the corresponding changes in electrical conductivity.

2. EXPERIMENTAL

The ceramic powder used throughout this work was a commercial α-Al_2O_3 (99.97 % pure RC-HP-DBM Baikowski Malakoff Industries, Inc., Reynolds, USA) whose density was taken as 3.98 g/cm^3. Distilled water was used as suspending liquid (measured average conductivity of 1.0 μS/cm; viscosity assumed to be 0.891 mPa.s at 25 °C, from the literature).

Particle morphology was observed by scanning electron microscopy (SEM, Leica Stereoscan 440). The particle size distribution was determined by static light scattering (Beckman-Coulter LS 230 Particle Size Analyzer).

Concentrated suspensions (35 vol.% solids, pH=6) were first purified from foreign ions by combined dialysis under slow magnetic stirring using ion exchanger beads (Merck Amberlite MB 6113 resin beads enclosed in Roth Nadir cellulose membrane dialysis tubing, with 50 mm diameter and 2.5-3.0 nm average pore size). Further details on the procedure can be found elsewhere [22]. Those dialysed suspensions showed no signs of sedimentation, even after rest periods as long as six months.

From the dialysed suspensions, very diluted ones were prepared (0.004 vol.% solids, at pH=6) to determine the average particle size. The hydrodynamic particle diameter *HD* was calculated using the Stokes-Einstein equation, $HD = k_B T / (3\pi\eta D_0)$. The particle diffusivity D_0 was determined by the Doppler effect in dynamic light scattering (DLS, Beckman-Coulter Delsa 440SX). A detailed description of the measuring principle can be found in the literature [10, 23]. The average particle size was also calculated as an equivalent spherical diameter from specific surface area (SSA) measurements (N_2 adsorption 5-point BET, Micromeritics Gemini 2370) and density.

After dialysis, the desired ionic strength was obtained by adding the appropriate amount of KCl (Merck, Germany) and the suspensions solids contents were adjusted back to the specified value (35 vol.% solids) by adding the appropriate amount of the corresponding suspending liquid (*i.e.* with the same ionic strength). KCl dissociates completely in water, its hydrolysis behaviour is little sensitive to the pH of the liquid and the two ions (K^+ and Cl^-) have similar ionic mobilities (respectively 7.62 and 7.91×10^{-8} m^2/sV) [23]. The concentration range used (0–90 mM) enabled the variation of the electrical conductivity of suspensions from 132 to 5730 µS/cm. A calibration curve (electrical conductivity *vs.* salt concentration) was constructed with KCl solutions in the same concentration range and then used to translate the suspensions measured conductivity values into effective ion concentration. That enables the calculation of the particles double layer actual thickness κ^{-1} (or Debye length) in each case [24]. Further details on the characterization of the suspensions electrical conductivity behaviour can be found elsewhere [21].

Electrical conductivity and pH measurements were carried out using the appropriate set of electrodes (WTW GmbH, Germany, TetraCon 325/inoLab, Cond Level2 at 400 Hz, and SenTix HW/inoLab, Ion Level2, respectively). ζ-potential was calculated from electrophoretic (static) mobility on very diluted suspensions (0.004 vol.% solids) in the pH range of 3–12 (Laser-Doppler-Electrophoresis, Beckman-Coulter Delsa 440SX). In the calculations, the Helmholtz-Smoluchowski model was used [21, 24]. As before, KCl was added to vary the ionic strength.

The rheological behaviour of suspensions was investigated at 25 °C in rotational tests with a shear stress-controlled rheometer (Thermo-Haake RS600). Possible wall-slip was investigated with a cone-and-plate geometry, in titanium and stainless-steel, and different surface finishes (polished and sand-blasted). No significant differences were observed in the resulting curves. Henceforth, the stationary measurements were carried out using a double gap measuring geometry (DG41) and a shear stress exponential increase from 0.01 to 100 Pa in 3 min. For each measurement, the values obtained for three consecutive tests were averaged and considered valid (*i.e.* confirmed steady state) only when the difference among them and the average was less than 1%. Liquid evaporation during measurements was avoided with the use of a solvent trap. Each flow curve was obtained (and compared) for three different samples with the same ionic strength.

3. RESULTS AND DISCUSSION

3.1. Particle characterization

Fig. 1 shows the particle size distribution (volume) as determined by static light scattering, suggesting an essentially monomodal distribution with a mean particle diameter (D_{50}) of 376 nm (particle radius a = 188 nm). The in-set in Fig. 1 illustrates the characteristic angular shape of the α-Al_2O_3 particles after the combined dialysis and surface cleaning process, as seen by scanning electron microscopy (SEM), and shows that, in average, particle size is ~200 nm. Both techniques are regarded as standard in the determination of particle sizes, but it is clear that the results can deviate substantially. Light scattering–based techniques tend to be preferred because they also provide information on the particle size distribution, which can be relevant if particle packing effects are to be considered later. However, those techniques also tend to over–estimate the particle size and favour larger particles (the intensity measured in

the light scattering method is proportional to D^6 [25] and, therefore, few large particles have a much greater volume impact than many small particles).

Rheology studies traditionally make use of a constant (average) particle size to simplify the flow modelling and, frequently, favour the particle hydrodynamic diameter (*HD*), also obtained from light-scattering (dynamic) measurements. If, for hard spheres, it is reasonable to consider the particle *HD* constant, typically that corresponding to the peak value in the differential size distribution, the same cannot be said about particles that can develop double layers. In such cases, as discussed earlier, the development of the electrical double layer is affected, just like the suspensions flow, by the particles' hydrodynamics, surface roughness and charge, and packing, all of which depend on and are related to the particles surface. Then, the average (spherical equivalent) particle size calculated from specific surface area (SSA) measurements [20] might be a better choice, suspended particles being still regarded as equivalent to a system of hard, smooth and monomodal particles. In the present work, the average particle size calculated from the measured SSA = 9.06 m^2/g resulted in a particle diameter of 166 nm, hence, a lower particle radius a_s = 83 nm.

The concern about the measurement accuracy of particle size and the significance of the electrical double layer thickness can be evidenced by the changes observed in the particles *HD* (curve (a) in Fig. 2), in comparison with the corresponding changes in ζ-potential (curve (b) in Fig. 2). The numbers shown next to the experimental data points in the ζ-potential curve in Fig. 2 are the corresponding κa values calculated using the SSA average particle size a_s = 83 nm and the κ^{-1} values for the measured suspension electrical conductivity, as obtained from the electrical conductivity *vs*. KCl concentration calibration curve (κ^{-1} is the Debye length and represents the double layer thickness). It might be worth remembering that for dilute suspensions of particles with thick double layers $\kappa a \approx 1$. Increasing ionic strength in the suspending liquid results in the compression of the diffuse layer and, hence, in the increase of the κa values [7, 21].

Fig. 2 shows that over the broad conductivity range investigated, ζ-potential presents a comparatively mild change (first increases up to a maximum of +89.2 mV to decrease again and then slowly approaches a value of +67.0 mV). However, significant changes do occur in the measured average particle *HD* and four different trends can be observed.

Initially, as the liquid conductivity increases, the fully extended double layers shrink due to the adsorption of counterions that lose their hydration entourage and the *HD* decreases sharply from 389 to 292 nm (for Cl^- ions (or K^+), dehydration corresponds to a reduction in radius from 0.33 to 0.18 nm) [23]. In this conductivity range (K < 218 μS/cm, $\kappa a < 10$) the observed increase in ζ-potential is nearly the same as the observed decrease in *HD* (~ 24 %), which suggests that the ζ-potential increase is the result of the reduction of the hydrodynamic friction forces (it should be reminded that ζ-potential is calculated from electrophoretic mobility) due to the reduction in the *HD*.

Next, for 218 μS/cm < K < 597 μS/cm ($10 < \kappa a < 20$), the *HD* curve shows a plateau (294 ± 2nm), while ζ-potential decreases markedly. Given that both hydrated ions and water molecules have similar hydrated radii (0.33 nm and 0.28 nm, respectively) [26], this shows that the spatial arrangement of the hydrated molecules that form the Stern layer is not being affected by the continuous increase of ions. For the suspensions in this low conductivity range, a nearly constant *HD* can indeed be assumed, which corresponds to a particle radius a_{HD} = 147 nm. Still, this is yet another different particle size, lying somewhere in between those obtained from static light scattering and SSA measurements (respectively, a = 188 nm and a_s = 83 nm).

Then, for 597 μS/cm < K < 2885 μS/cm ($20 < \kappa a < 39$), an increase in *HD* is observed, likely due to the attraction and accumulation of hydrated co- and counterions in the diffuse layer. The simultaneous slower decrease in ζ-potential can be explained by the completion of the Stern layer beyond 597 μS/cm, which corresponds to the secondary minimum of the DLVO theory [21]. Ions surrounding the particles reduce ζ-potential but, above all, limit the extension of the double layers, as expected from the DLVO total interaction potential. Given the reduction in the interaction distance between particles, partial agglomeration (formation of duplets) might be occurring during this increase in the charge density on the particle surface.

Finally, for 2885 μS/cm < K < 3822 μS/cm ($39 < \kappa a < 50$), the *HD* jumps from 344 to 466 nm (35 %) while ζ-potential falls, but only by 9.5 %. That decrease in ζ-potential can be explained by the collapse of the electrical double layer, which limits its effect to a few nanometers. Under varying ionic strength, the thickness of the hydrodynamic layer is, therefore, hardly coincident with that of the electrical double layers and the fall in ζ-potential alone cannot explain the sharp increase in *HD*.

Considering that ζ-potential is calculated from mobility values and mobility itself is expected to be controlled, at least in some extent, by the change in *HD*, the findings just described show that the general acceptance of ζ-potential as the sole criterion for suspension stability can be rather deceptive. This also shows that the common neglect of the variability of the electrical double layer thickness in response to changes in ionic strength in the study of suspensions flow can be a gross approximation.

3.2. Rheological behaviour under stationary conditions

The effect of the changes in ionic strength (due to changes in the added salt content) on the general characteristics of the α-Al_2O_3 suspensions (constant solids volume fraction $\phi = 0.35$) was investigated. Similarly to what was observed for electrical conductivity and zeta potential measurements [21], the variation in the ion concentration in the suspending liquid causes profound changes in the suspensions' rheological response (Fig. 3; to avoid overcrowding and for the sake of clarity, only representative curves are plotted).

The Péclet number (*Pe*) for the entire shear rate range is also shown in Fig. 3 along with the experimentally determined flow curves so that the influence of other variables on the flow behaviour might be ascertained. The poor agreement between the *Pe* line and any of the flow curves can be readily seen, which means that the dimensionless number description of the flow is inappropriate and demonstrates the prevalence of the effects other than the hydrodynamic or thermal ones.

All suspensions displayed a non-Newtonian behaviour while the suspension electrical conductivity K_S was varied from 132 to 5730 μS/cm. Nevertheless, two different behaviours could be distinguished with the increase in conductivity: a decrease in viscosity for dispersed suspensions with low ion concentrations and conductivities (132 μS/cm < K_S < 895 μS/cm), shown in Fig. 3 (a); and an increase in viscosity for coagulated suspensions with high ion concentrations and conductivities (1200 μS/cm < K_S < 5730 μS/cm), shown in Fig. 3 (b).

For all dispersed suspensions with low conductivity, shown in Fig. 3 (a), the shear stress increases steadily with the shear rate (viscous behaviour with no apparent yield stress; a strong effect on the initial flow can only be seen for 132 μS/cm). As the conductivity increases (*e.g.*, 132 compared to 895 μS/cm), the flow curve tends to a nearly Newtonian flow behaviour (liquid-like constant slope) and shows decreasing shear-thinning. This has been attributed to a prevalence of long-range repulsive electrostatic interparticle forces, leading to

the formation of a periodic structure that progressively weakens and collapses at high shear rates (approximately for $\dot{\gamma} > 1000\ s^{-1}$), when all flow curves appear to converge [11, 19]. In other words, for those high shear rates, suspended particles behave like hard spheres (*i.e*. no particle interaction) and the apparent viscosity becomes independent of the shear rate and constant for all suspensions investigated.

For suspensions with high ion concentration and high conductivity, Fig. 3 (b) shows two clearly different behaviour regions, one for low shear rates ($\dot{\gamma} < 0.01\ s^{-1}$) and another for high shear rates ($\dot{\gamma} > 1.0\ s^{-1}$). In the low shear rate region, coagulated suspensions ($K_S > 1808$ μS/cm) behave like a plastic body and ease shear by deforming. The plastic stress range increases (higher flow limit or yield stress) as the suspension conductivity increases and some "slip-stick" behaviour can be seen at the beginning of the curves, as the suspension resists deformation. This behaviour has been attributed to the existence within the suspension, as the ion concentration increases in the suspending liquid, of a progressively stronger percolative structure resulting from attractive electrostatic interparticle forces [11, 19].

The second region, of high shear rates, corresponds to the suspensions' actual flow, which occurs abruptly as a "landslide" once they overcome their respective yield stress. After that, the suspensions appear to behave just like low shear-thinning fluids that tend to constant viscosity. The flow curve for the suspension with $K_S = 1200$ μS/cm lies entirely in this region and resembles the curve for $K_S = 895$ μS/cm in Fig. 3 (a). For the other suspensions of increasing conductivity and higher flow limit (or yield stress), the transition to this behaviour requires successively higher shear stresses. Although all flow curves appear to converge at high shear rates (approximately for $\dot{\gamma} > 1000\ s^{-1}$), they remain well away from the *Pe* line.

The flow curves for 1808 and 2150 μS/cm are nearly coincident and these suspensions are those that show first signs of plastic behaviour, hinting at the existence of a percolation limit at which the attractive forces are just strong enough to hold the particles in the structure.

To better visualize the differences between the types of forces that influence the particles and determine the suspension's structure, attention is drawn to typical curves corresponding to a periodic structure ($K_S = 132$ μS/cm in Fig. 3-a) and a percolative structure ($K_S = 2150$ μS/cm in Fig. 3-b). The dispersed suspension curve for $K_S = 895$ μS/cm (in Fig. 3-a), with a nearly Newtonian (liquid-like) flow behaviour, can also be used in the comparison.

Both periodic and percolative suspensions require a similar shear rate ($\dot{\gamma} \approx 2x10^{-3}$ s^{-1}) to display any resistance (measurable stress). In the periodic suspension (K_S = 132 μS/cm, dominating repulsive forces) the structure is able to adjust to the increase in the shear stress and align with the stress field, that is, the particles are displaced from their equilibrium position but remain in a structure that is retained over a broad shear range. This stabilization effect is known as secondary electroviscous effect [11]. For this suspension, particle interactions prevail over shear forces in the whole shear rate range, *i.e*. the double layer effects are always present and can be measured. On the contrary, the rigid percolative structure in the coagulated suspension (K_S = 2150 μS/cm, dominating attractive forces) is easily ruptured and collapses with a small increase in the shear stress: the suspension soon displays a liquid-like flow. Nevertheless, given a high enough shear rate, both curves tend to the flow behaviour displayed by the dispersed suspension (K_S = 895 μS/cm) that stands as a barrier that neither the percolative nor the periodic suspensions can overtake.

Flow curves are usually presented in terms of apparent viscosity η as a function of shear rate, as shown in Fig. 4. As mentioned before, these curves are but a mathematical artefact and not the representation of the true viscosity (slope of the τ *vs*. $\dot{\gamma}$ curve).

The first point to note in Fig. 4 is that when the electrical conductivity increases, the apparent viscosity first decreases, as seen in Fig. 4 (a), and then increases again, as in Fig. 4 (b), and the suspensions present a viscosity minimum for 895 μS/cm < K_S < 1200 μS/cm. It should also be observed in Fig. 4 (a) that the zero-shear viscosity (η_0) is very sensitive to electrical conductivity variations: roughly, it varies three orders of magnitude, *i.e*. 0.01 Pa.s < η_0 < 10 Pa.s. In all cases the viscosity at high shear (η_∞) appears to be independent of the conductivity and seems to approach a constant value (~ 0.006 Pa.s, also shown by the dash-dotted lines in Fig.s 4-a and 4-b) as expected for the hard sphere model (*i.e*. no particle interaction). This is a clear indication of the dominance, in this shear range, of hydrodynamic forces. The difference between zero and infinite shear viscosities ($\Delta\eta = \eta_0 - \eta_\infty$) is frequently used to characterize the shear-thinning degree. These two viscosities are also commonly used to define a critical, or characteristic, viscosity $\eta_{char} = (\eta_\infty+\eta_0)/2$ to which corresponds a shear rate $\dot{\gamma}_{char}$ that represents the flow [27].

The overall shape of the curves in Fig. 4, both (a) and (b), would, at first glance, point at a shear-thinning behaviour limited between well defined (shear rate independent) low and high shear viscosity values (respectively, η_0 and η_∞). However, although the viscosity at the

"landslide" (yield viscosity, η_y) is even more sensitive to electrical conductivity variations, the shear-thinning behaviour in Fig. 4 (b) is really limited to the high shear range after the structural rupture, corresponding to only one order of magnitude variation for the "zero-shear viscosity" (*i.e.* 0.01 Pa.s < η_0 < 0.1 Pa.s).

Fig. 5 evidences how the particle interactions, hence, the suspension electrical conductivity K_S affects the way suspension flow begins (η_0 for low conductivity suspensions, and the viscosity at the "landslide", η_y, for high conductivity suspensions). For suspensions with predominantly repulsive forces (132 μS/cm < K_S < 895 μS/cm) as those shown in Fig. 4 (a), the initially extended double layers keep the particles restrained in a repulsive structure, each particle having little manoeuvrability. As the conductivity of the suspension increases, the double layers shrink and the repulsive forces decrease, which enables reduced particle interaction. Thus, as shown by the dotted straight line in Fig. 4 (a), measurement of η_0 at a constant shear stress τ = 0.01 Pa requires successively higher shear rates and its value decreases (less stiff particle structure), as seen in Fig. 5.

These low conductivity suspensions behave like viscoelastic liquids and the continuous drop in the apparent viscosity with increasing shear rate represents a true shear-thinning behaviour, which has been explained by a repulsive (periodic) structure that tends to align almost immediately with the shear field for each increment in the shear rate. When the conductivity of the suspension increases and the particle mobility increases, the structure adjustment to the shear field gets easier and faster and the suspensions flow with less resistance approaching Newtonian behaviour: the shear-thinning degree ($\Delta\eta = \eta_0 - \eta_\infty$) decreases.

The progressive addition of salt causes a deep change in the rheological properties of the suspensions, undoubtedly due to changes in the suspension structure. For suspensions with predominantly attractive forces (1200 μS/cm < K_S < 5730 μS/cm) as those shown in Fig. 4 (b), as the added ions that promote the shrinkage of the electrical double layer allow the attractive forces to take over, the agglomerated particles are held in a connecting (percolative) structure that becomes stronger. Consequently, the yield viscosity, η_y, sharply increases, as shown in Fig. 5. Although an apparent viscosity can be calculated, there is no actual flow, only the presence of a solid-like structure that can sustain a finite increasing stress before yielding and deforming plastically [7]. When the interparticle and hydrodynamic forces balance each other, the percolative structure abruptly breaks (as a "landslide") and flow occurs at a nearly constant stress, as seen in Fig. 3 (b) and described by the nearly parallel η

vs. $\dot{\gamma}$ lines inclined at ~ -45° in Fig. 4 (b). Although the flow curves in Fig. 4 (b) could easily be misconstrued as shear-thinning, this is typical of plastic flow (*i.e*. with a clear flow limit), both Bingham and non-linear.

Such changes can be better observed in Fig. 6, which highlights the existence of the typical yield stress (flow limit) for coagulated systems and the accompanying abrupt viscosity drop. Fig. 6 also evidences how henceforth the flow occurs as shear-thinning. If compared back to that observed in Fig. 4 (a), the true shear-thinning degree of these high conductivity suspensions (K_S > 1200 μS/cm) is much smaller, less than one order of magnitude. However, the values of the yield and infinite shear viscosities can be used to define the suspension's yield stress τ_y as the one that corresponds to $(\eta_y+\eta_\infty)/2$.

As already commented, the yield stress increases as the interparticle bonds strengthen with the increase in suspension conductivity. Before the yield stress is reached, the applied shear pushes particles to slip past each other, but it is not enough to keep them apart and so, they stick back. In other words, there is a competition between destruction and reconstruction of agglomerates. The rigid elasto-plastic suspension structure remains stable as long as the deformation rate does not give rise to a stress that exceeds the interparticle forces.

As the conductivity increases, the fluctuations in η_y ("slip-stick" motion within agglomerated particles) get wider and the effect is more persistent (extends to higher shear stresses). Apparently, the particle structure can be deformed further before rupturing, which obviously has to do with the interparticle forces. Once the hydrodynamic forces overtake the attraction forces and the structure collapses, which, as seen in Fig. 3 (b), occurs at higher shear rate for higher ionic strength, the liquid enclosed in the agglomerates is made available and, as in a "landslide", the shear stress becomes nearly independent of $\dot{\gamma}$. After the abrupt lowering of the apparent viscosity seen in Fig. 6, all suspensions flow in a similar low shear-thinning way. This behaviour seems similar to what was observed for the low conductivity (dispersed) suspensions. However, for these high conductivity suspensions the viscosity at high shear (η_∞) appears to be affected by the ionic strength (*i.e*. salt concentration) and no longer approaches the same constant value: as the conductivity increases, a shallow viscosity minimum can be observed, which shifts to higher values as well as to higher shear stresses. This might be a direct consequence of the change in the viscosity of the suspending liquid, due to the increasing salt concentration.

The flow behaviours described above have been observed frequently but usually associated with suspensions of varying solids contents [9]. As such, changes in the suspensions' structures were proposed and interpreted as a consequence of those varying solids contents. Given that, in the present work, the solids content was kept constant in all experiments (ϕ = 0.35), the two very different flow behaviours that could be identified just by varying the ionic strength must still stem from the corresponding different structures. In other words, despite the same solids content different structures are produced, the viscous (shear-thinning) behaviour observed for low ionic strength resulting from periodic structures and the non-linear plastic behaviour with a clear yield stress observed for high ionic strength resulting from percolative structures.

This confirms recent literature [21] that showed how the changes in ionic strength have a direct bearing on the changes in the suspensions' electrical conductivity through the effect on the particle electrical double layers and the DLVO interparticle forces. Despite the proven dominance of the electrostatic interactions over the Brownian motion and the applied shear, an explanation based on the developed interparticle forces still has to be sought for those different structures, as well as for the transition from one type of behaviour to the other, *i.e.* from Fig. 4 (a) to Fig. 4 (b). It has been shown that the suspensions conductivity is extremely sensitive to the presence of the particles [21] and it is envisioned that electrical conductivity measurements might provide the means to pinpoint when (*i.e.* for which ionic strength) the particle double layers touch or overlap, or stop doing so, and which effects influence the suspension structure.

3.3. Mathematical description of stationary measurements

The Carreau-Yasuda model (Eq. 1) is commonly chosen to describe the asymptotic (power law) shear-thinning flow behaviour of suspensions with no obvious yield stress, between a constant zero-shear viscosity (η_0) and an also constant viscosity at infinite shear rate (η_∞):

$$\frac{\eta - \eta_0}{\eta_0 - \eta_\infty} = \left[1 + (\theta\dot{\gamma})^{\alpha}\right]^{(n-1)/\alpha} \quad \text{(Eq. 1)}$$

In Eq. 1 θ is a constant with time dimensions and θ^{-1} represents the shear rate from which onwards the shear-thinning flow can be described by the power law (*i.e.* viscosity begins to decrease). The parameter α represents the width (shear range) of the constant η_0 region before the power law domain and (n-1) is the power law slope in a bi-logarithm representation. Eq. 1

was fitted to the experimental data for the flow curves of the suspensions with low conductivity plotted in Fig. 4 (a). The flow curve for the suspension with K_S = 1200 μS/cm, shown in Fig. 4 (b), was also included in the fitting to find out if the transition between structures could be detected. The parameters listed in Table 1 were obtained from the fitting.

Compared to the flow curves in Fig. 4 (a), Fig.s in Table 1 show that there is a good agreement between the calculated θ^{-1} and the shear rate value measured at the beginning of the shear-thinning flow, as well as between the calculated α values, which decrease as the conductivity increases, and the observed successively narrower shear range for constant η_0 at the beginning of the flow curves.

The shear-thinning degree ($\Delta\eta = \eta_0 - \eta_\infty$) is seen to go through a minimum for the suspension with electrical conductivity around 895 μS/cm, which indicates that the importance of the non-hydrodynamic forces is correspondingly decreasing. The increasing shear rate effect towards a common η_∞ reflects the dominance of the hydrodynamic forces over the electrostatic repulsive forces in the high shear rate range. This value coincides with that recorded experimentally, shown in Fig. 4, which was assumed as the viscosity $\eta_{\infty,HS}$ = 0.006 Pa.s for the hard sphere model.

As anticipated, the model fitting brought to evidence that the change of structure occurs somewhere in the K_S conductivity range 895 μS/cm < K_S < 1200 μS/cm. Those two flow curves can be compared going back to Fig. 4. Although both suspensions approach Newtonian behaviour, it can be seen that the flow curve for the suspension with higher ionic strength (K_S = 1200 μS/cm) tends to a lower η_∞. At the higher salt concentration the double layer is more compressed and its "repulsive" effect is completely overcome at high shear rate ($\dot{\gamma} > 10^4$ s^{-1}) by the hydrodynamic forces and $\eta_\infty \approx \eta_{\infty,HS}$. Given that the viscosity η_0 for K_S = 1200 μS/cm is higher than η_0 for K_S = 895 μS/cm, weak attractive forces may already be present in the former (weakly coagulated). This is characteristic of unstable suspensions and signals the beginning of the coagulation process (secondary attractive minimum of the DLVO total electrostatic potential curve) [21, 25].

As mentioned before, the shear-thinning flow can be represented by a characteristic (or critical) viscosity $\eta_{char} = (\eta_\infty+\eta_0)/2$, to which corresponds a characteristic shear rate $\dot{\gamma}_{char}$ [27]. The values obtained for the latter from those calculated for that critical viscosity are also listed in Table 1 and show that it depends on the electrical conductivity, increasing as it

decreases. Again, there is evidence of a change of structure occurring in the K_S conductivity range 895 μS/cm < K_S < 1200 μS/cm.

Despite the observed good fitting of individual flow curves, the classical rheology model described above does not add much to the understanding of the effects of the particles size and morphology, or of the presence of their electrical double layers, for that matter. In fact, it clearly suggests that the various suspensions behave as if they contained different solids loads. This, in turn, is a clear manifestation of the effect of the particles electrical double layer, which translates into different effective particle volume fraction ϕ_{eff} [12]. This concept is described by Eq. 2, for an original volume fraction ϕ of particles with radius a and undisturbed electrical double layer thickness (or Debye length) κ^{-1} and, clearly, requires precise measurements of a and κ^{-1}:

$$\phi_{eff} = \phi\left(1 + \frac{\kappa^{-1}}{a}\right)^3 \quad \text{(Eq. 2)}$$

As mentioned before, κ^{-1} is calculated for the salt concentration corresponding to the measured suspension conductivity using the electrical conductivity *vs*. KCl concentration calibration curve.

Table 2 presents and compares, for the dispersed suspensions shown in Fig.s 3 (a) and 4 (a) and in Table 1 (viscoelastic liquids with periodic structure), the values of ϕ_{eff} and the corresponding κ^{-1} calculated for a particle radius a = 188 nm, a_{HD} = 147 nm or a_s = 83 nm, as determined by static and dynamic light scattering and BET measurements, respectively.

The Krieger-Dougherty model for hard spheres [8, 9] is generally proposed to describe how the effective solids volume affects the relative zero-shear viscosity of the suspension ($\eta_{0,r} = \eta_0/\eta_{solution}$, calculated values also shown in Table 2; $\eta_{solution}$ = 0.891 mPa.s assumed constant and equal to that of distilled water at 25 °C). The model is expressed as in Eq. 3, in which ϕ_{eff} replaces ϕ and [η] is the intrinsic viscosity, which gives a measure of the particle morphological characteristics. Values for [η] have been reported ranging from 1.5 to 5 ([η] = 2.5 for a suspended single hard spherical particle) [28]:

$$\eta_{0,r} = \left(1 - \frac{\phi_{eff}}{\phi_{Max}}\right)^{-[\eta]\phi_{Max}} \quad \text{(Eq. 3)}$$

According to Eq. 3, when ϕ_{eff} approaches the maximum volume fraction ϕ_{Max}, $\eta_{0,r}$ tends to ∞ (*i.e*. solid-like behaviour). By fitting Eq. 3 to the experimental data, values of ϕ_{Max} and [η] are

obtained. Both the experimental data in Table 2 and the model curve (Fig. 7) show the expected increase in the relative viscosity with increasing effective solids volume fraction (or with the decrease of the suspension conductivity), but rather different sets of results are obtained depending on which particle size is used.

As shown by curve (a) in Fig. 7, for the particle radius a = 188 nm (determined by static light scattering) the parameters extracted from the Krieger-Dougherty calculated curve are ϕ_{Max} = 0.438 and [η] = 4.2 but the experimental data for low ϕ_{eff} values are inadequately represented by the model. Also, practical experience shows that even with a solids volume content near 60 %, stable suspensions normally still flow. Thus, a higher packing density ($\phi_{Max} > 0.50$) would be expected. The contribution of the intrinsic viscosity [η] = 4.2 is significantly higher than that expected for Einstein's spherical particles. This deviation can reasonably be mostly attributed to the powder's characteristics (the α-Al_2O_3 particles used are not smooth, have angular shape and a broad particle size distribution) and, above all, to the very high concentration of suspensions.

On the other hand, curve (c) in Fig. 7 shows that when the particle radius used is a_s = 83 nm, as determined from the measured specific surface area (and closest to that observed by SEM), a very good agreement is found between the model and the experimental data in the whole ϕ_{eff} range. In this case, the Krieger-Dougherty parameters are ϕ_{Max} = 0.575 and [η] = 4.3 and, clearly, $\phi_{Max,83nm} > \phi_{Max,188nm}$. For this particle size, ϕ_{Max} is between the simple cubic (0.524) and the random loose packing (0.600) [29]. This is evidence that the particles in this salt concentration range behave like hard spheres despite their thick electrical double layer (soft spheres).

Curve (b) in Fig. 7, constructed using the hydrodynamic radius a_{HD} = 147 nm lies in between the other two, with values of ϕ_{Max} = 0.462 and [η] = 4.3, as would be expected for an intermediate value of particle size. However, curve (b) lies closer to curve (a) and shows an equally bad fitting of experimental data in the low ϕ_{eff} range.

When the characteristic shear $\dot{\gamma}_{char}$ values obtained for the shear-thinning curves (Table 1) and the corresponding $\eta_{0,r}$ (Table 2) are plotted as in Fig. 8, a nearly linear relationship between the logarithms of $\eta_{0,r}$ and $\dot{\gamma}_{char}$ can be observed, corresponding to a power law dependence with the exponent of ~ -1. Fig. 8 could be regarded as a "master flow curve" for this family of dispersed α-Al_2O_3 low conductivity suspensions with constant solids fraction (ϕ

= 0.35). Using this normalization procedure, the different shear-thinning degrees observed in the curves in Fig. 4 (a) collapse into a single line that describes the flow behaviour of the family.

As the salt concentration decreases, the double layer thickness κ^{-1} increases. This reduces the average separation distance between the particles d_{SD} (Eq. 4) [30], so that the probability of a collision or overlapping of the electrical double layers increases. This shows that the observed strong shear-thinning behaviour arises from particle interaction and reflects the lack of long-range structure in dilute suspensions of hard spheres [7]. The rapid increase in the relative viscosity when ϕ_{eff} approaches ϕ_{Max} indicates that the particles average separation distance is then (*i.e.* for the lowest suspension conductivity) about twice as large as the electrical double layer ($d_{SD} \approx 2 \times \kappa^{-1}$) and their rearrangement will result in stored elastic energy:

$$d_{SD} = 2a\left[\left(\frac{\phi_{Max}}{\phi}\right)^{1/3}\right] \qquad \text{(Eq. 4)}$$

For a particle radius a = 83 nm, ϕ_{Max} = 0.575 and ϕ = 0.35, this results in a mean separation distance d_{SD} = 29.9 nm, which is to say that the double layer thickness would be $\kappa^{-1} \approx$ 14.9 nm. This value is comparable to the value of 14.2 nm calculated for the suspension with K_S = 132 µS/cm (Table 2). In other words, particles are tightly packed and this suspension is expected to behave like an elastic solid. Whether such suspension structure has an elastic character or not, can only be ascertained by means of non-stationary (oscillatory) measurements.

The above discussion has highlighted that both flow curve measurement and particle size determination can be sources of nagging interpretation of experimental data, fostered by the increasing use of automated measuring systems. The various representations of flow curves are but mathematical artefacts that can be seriously misleading if care is not taken to not overestimate the techniques' wisdom. Similarly, popular "push-button" techniques to measure particle sizes are prone to neglect the variability of the electrical double layer thickness in response to changes in ionic strength, which can result in a gross estimate of particle size. When the "right" particle size is considered, suspensions flow models of recognised undisputed value can be seen to hold true. Fortunately, in a vast majority of applications of high ionic strength, the shrunk electrical double layer can indeed be "ignored" and, therefore, those mathematical models can also ignore the particle size and remain valid.

This reasoning can be further illustrated by considering the suspensions with high conductivity (thin double layer), with a predominantly attractive particle structure and an apparent yield stress τ_y. For these suspensions, the Herschel-Bulkley model ($\tau = \tau_y + k_1 \dot{\gamma}^n$) was fitted to the flow curves shown in Fig. 3 (b). Given the close resemblance between the curves in the K_S range 1808 to 2150 μS/cm, only the latter was included in the fitting. The resulting fitting parameters are listed in Table 3.

Although it ignores the size of suspended particles, one of the advantages of the Herschel-Bulkley model is that it separates the contributions of the suspension's structure to the resistance to initial flow (yield stress) from that to the ensuing flow (shear rate power law). The increase in conductivity, which leads to the increase in the resistance during flow, seen in Fig.s 4 (b) and 6 and gauged by k_1 and n, also leads to a significant increase in the initial flow resistance (τ_y). Besides the formation of agglomerates (n <1), the increase in both τ_y and k_1 are indicative of a progressive strengthening of the percolative (coagulated) structure. Moreover, the much larger change in k_1 than that in n suggests that the effects of added ions are mostly felt on the colloidal ($\Delta k_1 \sim 450$ %) rather than on the viscous ($\Delta n \sim 8$ %) components of the suspension response (values of $n \approx 1$ characterize a nearly-Bingham flow). In other words, the interparticle forces were strengthened while the shape and size of agglomerates hardly changed. Naturally, the Herschel-Bulkley model is concerned with the flow itself and leaves out the changes clearly observed before τ_y, or in the corresponding yield viscosity η_y, seen earlier in Fig. 5. However, these are the changes that directly reflect the strength build up in the interparticle forces. The contribution of the added salt to the increase in τ_y might be understood with the aid of a stabilization theory, which will be discussed in the following section.

3.4. Stability of suspensions: DLVO theory, electrical conductivity and viscosity

The work of Cruz *et al*. on colloidal stability [21], relating the DLVO theory to the electrical conductivity of suspensions K_S, suspending liquids K and suspended particles K_P, can be used to further discuss the rheological properties and characterize the particles behaviour at certain electrolyte concentrations. Fig. 9 shows the observed changes in η_0 and η_y, as a function of the conductivity of the electrolyte (plotted earlier in Fig. 5 as a function of the suspensions conductivities), superposed with those of particle conductivity K_P (from Cruz *et al*. [21]).

Region I in Fig. 9 covers the initial important decrease in the zero-shear viscosity observed for suspensions containing low KCl concentrations and extends up to the isoconductivity point (ICP) between the particles and the suspending electrolyte (c_{KCl} = 1.89 mM, K = K_P = 277 μS/cm, κ*a* = 12, maximum ζ–potential).

For these low ionic strength suspensions, the particles display fully extended double layers and a very strong repulsive total interaction potential. As seen earlier, in a suspension with a solids volume fraction ϕ = 0.35 the particle spacing is only ~ 30 nm, while the repulsive potential begins to be felt at a distance above 100 nm (≈ 8 × κ^{-1}). For a suspension with c_{KCl} = 0.46 mM (K_S = 132 μS/cm), this corresponds to 85 % overlap of the double layers. That strong overlap is alleviated with the increase in the ion concentration, which explains the observed fast decrease in the viscosity.

From the literature [21], as the ionic strength (c_{KCl}) increases, the ICP occurs when the compression of the diffuse layer is about to begin, hence the contribution of the particles' shrinking electrical double layer to the suspension's conductivity loses weight. As such, the ICP also signals the point beyond which the ζ-potential experimental determination becomes less sensitive to external factors fluctuations and roughly separates the region in which the conductivity of the suspension is higher than that of the suspending liquid from the region in which it is lower than that of the suspending liquid.

After the ICP (region II in Fig. 9), although the particles' conductivity is still increasing towards $K_{P,Max}$, their less extended electrical double layers continue to shrink and the suspensions' viscosity continues to decrease, although more slowly, towards the desired minimum for ideal processing conditions.

The particles maximum conductivity (c_{KCl} = 3.5 mM, κ*a* = 16, K = 500 μS/cm and K_P = $K_{P,Max}$ = 335 μS/cm) occurs when the repulsive potential between particles is maximum ($V_{Tot,Max}$ = 282.4 k_BT, at ~ 1.5 nm) and the attractive minimum begins to form (-0.2 k_BT, at 46 nm) [21]. Although there is still some double layer overlapping, repulsion is still dominant and thermal movement is enough to break all particle-particle bonds, so the suspension remains stable. From then onwards, the interparticle distance can be shortened and decreasing effective particle volume fraction, or denser particle packing, is possible.

The DLVO theory predicts [21] that above this ion concentration (c_{KCl} > 3.5 mM) the depth of the secondary attractive minimum increases and it occurs at a shorter distance, while the

height of the repulsive maximum decreases. So, the suspension stability is determined by the balance between attractive and repulsive forces. That balance is reached when the particles conductivity is $K_{P,Eq}$ (c_{KCl} = 13.2 mM, κa = 34), when the repulsive maximum reaches ~127 k_BT and the closer (~17 nm) attractive secondary minimum reaches ~ -1.5 k_BT. The position of this secondary attractive minimum corresponds to a pair of particles that are on average 34 nm apart. A comparison with the calculated separation distance d_{SD} of 29.9 nm (Eq. 4) shows a very good agreement. At this condition, that marks the end of region II in Fig. 9, particles stand at an equilibrium distance, having the same probability of being attracted or repelled by the total interaction potential and the viscosity goes through a minimum (0.0134 Pa.s < η_0 < 0.0192 Pa.s observed for 11.1 mM < c_{KCl} < 16.0 mM).

As the ionic strength is increased past $K_{P,Eq}$, although the particle conductivity continues decreasing, the attractive forces become dominant and the viscosity increases and enters region III in Fig. 11. When K_P = 0 (c_{KCl} = 30.5 mM, κa = 47) the double layer is fully collapsed (repulsive maximum ~12 k_BT) and particles stand at the closest reversible distance (~7 nm, attractive minimum ~ -5 k_BT) [21]. This can be regarded as the critical ionic strength for coagulation, *i.e*. the interparticle distance is at the brim of the total potential primary minimum, which is felt as a slight inflection in the viscosity curve. The strong change in the stability of the suspensions at K_P = 0 reflects the formation of strong agglomerates, which results in the steep increase in η_y observed in Fig.s 5 and 9 and explains the "slip-stick" behaviour observed in Fig.s 3 (b) and 4 (b).

For higher ion concentrations (c_{KCl} > 30.5 mM), the charges on the particles surface are fully compensated by the counterions and the particles no longer conduct. The repulsive maximum tends to disappear while the secondary attractive minimum gets deeper, and the suspensions are destabilized by the attractive interparticle forces. That is, a percolative structure can be formed in the suspension only when all the charges of the particles have been compensated.

The DLVO total potential curves for the suspensions listed in Table 3 are plotted in Fig. 10 and clearly illustrate the changes in the position and magnitude of both the attractive and the repulsive peaks. Those curves are expressed as energy *vs*. distance (U *vs*. d) and, by calculating the corresponding derivative relative to distance (dU/dd), a measure of the interparticle force can be obtained (dU = F dd), also shown in Fig. 10. When the particles stand in equilibrium at the attractive minimum, they rest at a distance d_0 measured at the point where the force is null. Any applied shear stretches the interparticle bond to a new distance d

and the corresponding strain, $\Delta d/d_0$, gives rise to an increase in stress, proportional to the resulting interparticle force. Such increasing stress corresponds to that observed before τ_y in the flow curves in Fig. 4 (b). When the maximum in the derivative curve (maximum force) is reached, the bond ruptures and slip occurs. On a macro scale (*i.e*. more than a pair of particles), some of the ruptured bonds will reform, others won't (*i.e*. slip-stick). The particle structure is deformed in a way that could be regarded as non-linear elastic (or, perhaps, unelastic), but flow does not occur and the structure can withstand increasing shear. As the applied shear increases, so does the resulting shear stress and, eventually, a statistically relevant number of bonds remain broken, which leads to the "landslide" slip. The corresponding stress is the τ_y in the Herschel-Bulkley model and the maximum force in the derivative curve in Fig. 10 stands as a measure of it. Fig. 10 also shows that increasing salt contents (*i.e*. increasing conductivity) result in lower d_0 values and higher strains at the peak force, confirming that the particle structure in the suspension gets stronger and can be deformed further before rupturing, as anticipated from the flow curves.

According to these explanations, the particle conductivity K_P is a suitable parameter to characterize the stability of colloidal suspensions, as highlighted by Cruz *et al*. [21]. For the equilibrium particle conductivity, signalled in Fig. 9, the viscosity has a minimum. For higher particle conductivities (left of the minimum into region II) the repulsive potential is dominant and the suspension viscosity increases due to the increase in the repulsive forces, whereas for lower particle conductivities (right of the minimum into region III) the attractive potential is dominant and the suspension viscosity increases due to the increase of the attractive forces. The suspensions are described as "dispersed" in the first case and "reversibly coagulated" in the second. Both structures can be seen as "periodic" or "liquid-like", as has been shown by the stationary rheological measurements. Extremely clean suspensions such as those in region I, although dispersed, can be far too rigid and are not easy to process; heavily ion-loaded suspensions such as those in region III (after $K_P = 0$) are prone to the formation of agglomerates and are commonly described as flocculated.

4. CONCLUSIONS

This work describes the stationary rheological measurements of concentrated α-alumina suspensions with constant solids content ($\phi = 0.35$) and controlled ionic strength in the light

of studies already in the literature on the electrical conductivity of suspensions and particles, as well as on the static and dynamic electrokinetic particle mobility [21]. Considering that, for a given particle size, the thicker the electrical double layer, the larger the liquid volume that is excluded by the particles, the effective solids volume ϕ_{eff} and the relative viscosity $\eta_{0,r}$ were used in the Krieger-Dougherty model for hard spheres [8, 9]. Although the expected trend was observed, a very good agreement between the model and the experimental data was found only when the surface area equivalent particle radius a_s was used. The use of the "right" particle size enabled the reliable calculation of the solids maximum volume fraction ϕ_{Max} and the intrinsic viscosity and demonstrated that suspensions flow models of recognised undisputed value still hold true [11, 15, 16].

Depending on the salt concentration, and by varying the salt concentration alone, two different flow behaviours could be identified in the suspensions, similar to those usually associated with suspensions of varying solids contents and explained by changes in the suspensions' structures [9]. In the present case, the differences also resulted from the corresponding different types of structures: (i) viscous behaviour without an apparent yield stress at low salt concentration (periodic structures) and (ii) non-linear plastic behaviour at high salt concentration (percolative structures). In between the two, at average salt concentration, suspensions presented near Newtonian behaviour (liquid-like structures).

A solids fraction $\phi_{Max} = 0.575$ was determined, that is, the particles behave as hard spheres despite their thick electrical double layers (soft spheres). When the salt concentration decreases, the double layer thickness κ^{-1} increases and the mean separation distance between the particles, d_{SD}, decreases [30]. Only if the average distance of the particles is about twice the thickness of the electrical double layer, $d_{SD} \approx 2 \times \kappa^{-1}$, can the suspensions store elastic energy due to the rearrangement of the particles.

For higher salt concentrations the suspensions behave as non-linear plastic liquids (percolative structure), displaying a structure viscosity with an apparent yield stress τ_y. Their flow curves could be described by the Herschel-Bulkley model, with increasing τ_y and k_1 as the suspension percolative (coagulated) structure gets progressively stronger [14, 17, 18]. This analysis evidenced that the increase in salt concentration particularly affects the colloidal rather than the viscous response of the suspension, *i.e.* the interparticle forces increased while the shape and size of agglomerates hardly changed, which was confirmed by the use of the DLVO total potential curves.

The existence of those three different suspension structures (periodic, liquid-like and percolative) was related to a particular equilibrium particle conductivity $K_{P,Eq}$, which was found to be in very good agreement with the DLVO theory and corresponds to a kinetic stability of colloidal suspensions: at this condition the particles are at an equilibrium distance, having the same probability of being attracted or repelled by the total interaction potential [21]. The relative viscosity has a minimum at $K_P = K_{P,Eq}$ and increases for $K_P < K_{P,Eq}$ due to the increase in the attractive forces (reversibly coagulated suspensions) and for $K_P > K_{P,Eq}$ due to the increase in the repulsive forces (dispersed suspension).

This work also highlights another rather important point, which is that, in the urge of using state-of-the-art powerful experimental techniques, or of generating new, more intricate, numerical simulation models, what might be hastily dismissed as "noise" because it can often be accommodated within the experimental error, is actually a (re)confirmed behaviour, with a sound physical interpretation. In the results discussed above, the electroviscous effect observed in viscoelastic concentrated suspensions finds support in oscillatory rheology measurements (a subject for a forthcoming paper). This broadens the understanding of suspensions stability and rheology, with strong bearings in colloidal suspensions manipulation and consolidation methods, namely for nanofluids and nanoparticles electrical conductivity [31].

ACKNOWLEDGEMENTS

Authors appreciate the financial support received from the Brazilian Research Agency CAPES (R.C.D. Cruz, Ph.D. grant) and from Deutsche Forschungsgemeinschaft (DFG Research Unit FOR 371).

REFERENCES

[1]. Willenbacher, N., Georgieva, K. Rheology of disperse systems, in Product Design and Engineering: Formulation of Gels and Pastes (eds U. Bröckel, W. Meier, G. Wagner), Wiley-VCH, Weinheim, Germany, 2013. DOI: 10.1002/9783527654741.ch1

[2]. Einstein, A., Eine neue Bestimmung der Moleküldimension, Ann. Phys. 19 (1906) 289–306. DOI: 10.1002/andp.19063240204

[3]. Derjaguin, B.V., Landau, L., Theory of the Stability of Strongly Charged Lyophobic Sols and of the Adhesion of Strongly Charged Particles in Solutions of Electrolytes, Acta Physicochim. 14 (1941) 633–661.

[4]. Verwey, E.J.W., Overbeek, J.Th.G., Theory of the Stability of Lyophobic Colloids, Elsevier, Amsterdam, 1948 (Also available as a Dover reprint, 1999).

[5]. Dobiáš, B. (Ed), Coagulation and Flocculation: Theory and Applications, Surfactant Science Series 47, Marcel Dekker, New York, 1993.

[6]. Sonntag, H., Strenge, K., Vincent, B., Coagulation Kinetics, in B. Vincent (Ed) Coagulation Kinetics and Structure Formation, Springer, Boston, MA, 1987. DOI: 10.1007/978-1-4757-0617-8_4

[7]. Russel, W.B., Structure-Property Relations for the Rheology of Dispersions of Charged Colloids, Ind. Eng. Chem. Res. 48 (2009) 2380–2386. DOI: 10.1021/ie800385m

[8]. Krieger, I.M., Rheology of polymer colloids, in Polymer Colloids, R. Buscall, T. Corner, J.F. Stageman (Eds), Elsevier, N.Y., 1985.

[9]. Quemada, D., An overview of recent results on rheology of concentrated colloidal dispersions, Progr. Colloid. Polym. Sci. 79 (1989) 112–119.

[10]. Larson, R.G., The structure and rheology of complex fluids, Vol. 150, Oxford University Press, New York, 1999.

[11]. Mewis, J., Wagner, N.J. Colloidal suspension rheology, Cambridge Series in Chemical Engineering, Cambridge University Press, 2012.

[12]. Tadros, Th.F., Correlation of viscoelastic properties of concentrated dispersions with their interparticle interaction, Trends in Colloid and Interface Science III, Prog. Colloid Polym. Sci. 79 (1989) 120-127.

[13]. Schramm, G., A Practical Approach to Rheology and Rheometry, 2nd ed., HAAKE GmbH, Karlsruhe, 1998.

[14]. Pahl, M., Gleissle, W., Laun, H.W., Praktische Rheologie der Kunststoff und Elastomer, VDI, 1991.

[15]. Rhodes, M.J., Introduction to particle technology, Wiley, 2008.

[16]. Rahaman, M.N., Ceramic Processing, Second Edition, CRC Press, Boca Raton, FL, 2017.

[17]. Barnes, H.A., Hutton, J.F., Walters, K. (Eds), An introduction to rheology, Rheology Series, Vol. 3, Elsevier, Amsterdam, 1989.

[18]. Macosko, C.W., Rheology: Principles, Measurements and Applications, Wiley-VCH, New York, 1994.

[19]. Russel, W.B., Saville, D.A., Schowalter, W.R., Colloidal Dispersions (Cambridge Monographs on Mechanics), Cambridge University Press, Cambridge, 1989. DOI: 10.1017/CBO9780511608810

[20]. Parfitt, G.D., Dispersion of powders in liquids: with special reference to pigments (2nd ed), Appl. Sci. Publishers, London, 1973.

[21]. Cruz, R.C.D., Segadães, A.M., Oberacker, R., Hoffmann, M.J., Double layer electrical conductivity as a stability criterion for concentrated colloidal suspensions, Colloids and Surfaces A: Physicochem. Eng. Aspects 520 (2017) 9–16. DOI: 10.1016/j.colsurfa.2017.01.059

[22]. Cruz, R.C.D., Reinshagen, J., Oberacker, R., Segadães, A.M., Hoffmann, M.J., Electrical Conductivity and Stability of Concentrated Aqueous Alumina Suspensions, J. Colloid Interface Sci. 286 (2005) 579–588. DOI: 10.1016/j.jcis.2005.02.025

[23]. Atkins, P., Paula, J., Atkins' Physical Chemistry, 9th ed., Oxford University Press, New York, 2010.

[24]. Hunter, R.J., Introduction to colloid science, Oxford University Press, Oxford, U.K., 1993.

[25]. Lagaly, G., Schulz, O., Zimehl, R., Dispersionen und Emulsionen: Eine Einführung in die Kolloidik feinverteilter Stoffe einschließlich der Tonminerale, Springer-Verlag, Berlin, 1997.

[26]. Israelachvili, J.N., Intermolecular and surface forces, 3rd ed., Academic Press, Elsevier, 2011.

[27]. Nommensen, P.A., Duits, M.H.G., van den Ende, D., Mellema, J., Steady shear behavior of polymerically stabilized suspensions: experiments and lubrication based modelling, Physical Review E, 53[3] (1999) 3147–3154.

[28]. Mueller, S., Llewellin, E.W., Mader, H.M., The rheology of suspensions of solid particles, Proc. R. Soc. A 466 (2010) 1201–1228. DOI: 10.1098/rspa.2009.0445

[29]. Scott, G.D., Kilgour, D.M., The Density of Random Close Packing of Spheres, Brit. J. Appl. Phys. (J. Phys. D) 2 (1969) 863–866.

[30]. Hoffmann, A.C., Kevelam, J., Model for the Interparticle Surface Separation in Concentrated Mono- and Polydisperse Suspensions, AIChE J., 45 (1999) 285-290. DOI:10.1002/aic.690450209

[31]. Geng, Y., Khodadadi, H., Karimipour, A., Reza Safaei, M., Nguyen, T.K., A comprehensive presentation on nanoparticles electrical conductivity of nanofluids: Statistical study concerned effects of temperature, nanoparticles type and solid volume concentration, Physica A: Statistical Mechanics and its Applications, 542 (2020) 123432. DOI: 10.1016/j.physa.2019.123432

Fig. 1. Particle size volume distribution of the α-Al_2O_3 powder as determined by static light scattering. The in-set illustrates the particle morphology as seen by SEM.

Fig. 2. Effect of the conductivity of the suspending liquid on the measured hydrodynamic diameter of the α-Al_2O_3 particles (curve a) and on the corresponding ζ-potential (curve b). The κ*a* values calculated for an average particle size a_s = 83 nm are shown next to the experimental data points in the ζ-potential curve.

Fig. 3. Flow curves (shear stress τ as a function of shear rate $\dot{\gamma}$) and *Pe vs.* $\dot{\gamma}$ (dashed line) for α-Al_2O_3 suspensions (ϕ = 0.35): (a) dispersed with low conductivity (low ionic strength); and (b) coagulated with high conductivity (high ionic strength).

Fig. 4. Flow curves (apparent viscosity η as a function of shear rate $\dot{\gamma}$) of α-Al_2O_3 suspensions (ϕ = 0.35): (a) dispersed with low conductivity (low ionic strength), the dotted line corresponds to a constant τ = 0.01 Pa; and (b) coagulated with high conductivity (high ionic strength). The dash-dotted lines represent the viscosity for no particle interaction ($\eta_{\infty,HS}$ for the hard sphere model).

Fig. 5. Effect of the conductivity of the suspensions K_S on the apparent viscosity at the onset of the flow for α-Al_2O_3 suspensions (ϕ = 0.35): η_0 for dispersed suspensions with low conductivity (low ionic strength); η_y for coagulated suspensions with high conductivity (high ionic strength).

Fig. 6. Flow curves (apparent viscosity η as a function of shear stress τ) for coagulated α-Al_2O_3 suspensions (ϕ = 0.35) with high conductivity (high ionic strength).

Fig. 7. Effect of the effective solids volume fraction on the relative viscosity of dispersed α-Al_2O_3 suspensions (ϕ = 0.35) and on calculated Krieger-Dougherty fitting curves, for a = 188 nm (curve a), a_{HD} = 147 nm (curve b) and a_s = 83 nm (curve c).

Fig. 8. Effect of the characteristic shear rate $\dot{\gamma}_{char}$ on the relative viscosity of dispersed α-Al_2O_3 suspensions (ϕ = 0.35) with low conductivity.

Fig. 9. Effect of the conductivity of the suspending liquid K on the apparent viscosity η_0 and η_y of α-Al_2O_3 suspensions (ϕ = 0.35), dispersed and coagulated (curve a), and on the suspended particles conductivity (curve b, from Cruz *et al*. [21]).

Fig. 10. DLVO total potential curves and corresponding derivatives for the α-Al_2O_3 suspensions (ϕ = 0.35) listed in Table 3, showing the effect of increasing added salt (*i.e*. increasing conductivity) on the stress induced by applied shear before τ_y.

Table 1. Calculated parameters (η_0, η_∞, θ, n, α) of the Carreau-Yasuda model for dispersed α-Al_2O_3 suspensions (ϕ =0.35) with low conductivity (low ionic strength).

K_S [µS/cm]	η_0 [Pa.s]	η_∞ [Pa.s]	θ [s]	n	α	θ^{-1} [s^{-1}]	$\Delta\eta$ [%]	$\dot{\gamma}_{char}$ [s^{-1}]
132	12.270	0.006	76.29	0.3315	2.047	0.013	100.0	0.04
172	0.151	0.006	3.544	0.5757	1.742	0.282	96.0	1.37
297	0.035	0.006	0.5164	0.6075	1.265	1.936	82.6	9.71
450	0.020	0.006	0.1516	0.4607	0.848	6.596	70.0	14.70
895	0.013	0.006	0.1453	0.4794	1.253	6.882	53.7	23.57
1200	0.019	0.006	0.2598	0.3285	0.550	3.849	69.3	1

Table 2. Calculated ϕ_{eff}, particle double layer thickness κ^{-1} and relative viscosity $\eta_{0,r}$ for dispersed α-Al_2O_3 suspensions (ϕ =0.35) with different conductivities K_S, as a function of particle radius a, a_{HD} and a_s.

			ϕ_{eff}			
K_S [µS/cm]	c_{KCl} [mM]	κ^{-1} [nm]	a = 188 nm	a_{HD} = 147 nm	a_s = 83 nm	$\eta_{0,r}$ [Pa.s]

132	0.460	14.2	0.435	0.462	0.561	13771
172	0.832	10.6	0.412	0.431	0.501	169.5
297	1.994	6.8	0.389	0.401	0.443	38.7
450	3.880	4.9	0.378	0.386	0.415	22.4
895	11.098	2.9	0.366	0.371	0.388	15.0

Table 3. Calculated parameters (τ_y, k_1 and n) of the Herschel-Bulkley model for coagulated α-Al_2O_3 suspensions (ϕ =0.35) with high conductivity (high ionic strength).

sK_S [μS/cm]	τ_y [Pa]	k_1	n	c_{KCl} [mM]
1200	0.001	0.006	0.984	16.0
2150	0.019	0.013	0.949	31.5
2600	1.387	0.017	0.915	38.7
5730	7.538	0.033	0.907	89.4

CRediT author statement

Robinson C. D. Cruz: Conceptualization, Investigation, Data Curation, Formal analysis, Methodology, Validation, Visualization, Writing - Original Draft

Ana M. Segadães: Methodology, Visualization, Writing - Review & Editing

Pedro Q. Mantas: Visualization, Formal analysis, Writing - Review & Editing

Rainer Oberacker: Conceptualization, Methodology, Resources, Supervision

Michael J. Hoffmann: Conceptualization, Methodology, Resources, Supervision

☒ The authors declare that they have no known competing financial interests or personal relationships that could have appeared to influence the work reported in this paper.

☐The authors declare the following financial interests/personal relationships which may be considered as potential competing interests: